EUROfusion

EUROFUSION WPJET1–PR(15)31

N. Den Harder et al.

ELM–Resolved Divertor Erosion in the JET ITER–Like Wall

Preprint of Paper to be submitted for publication in
Nuclear Fusion

This work has been carried out within the framework of the EUROfusion Consortium and has received funding from the Euratom research and training programme 2014-2018 under grant agreement No 633053. The views and opinions expressed herein do not necessarily reflect those of the European Commission.

ELM-resolved divertor erosion in the JET ITER-Like Wall

N. Den Harder,[1,2] S. Brezinsek,[1] T. Pütterich,[3] N. Fedorczak,[4] G.F. Matthews,[1] A. Meigs,[1] M.F. Stamp,[1] M.C.M. van de Sanden,[2] G.J. Van Rooij,[2] and JET Contributors[5]
[1)] *EUROfusion Consortium, JET, Culham Science Centre, Abingdon, OX14 3DB, United Kingdom*
[2)] *FOM Institute DIFFER Dutch Institute for Fundamental Energy Research, Partner in the Trilateral Euregio Cluster, the Netherlands, www.differ.nl*[a)]
[3)] *IPP - Max-Planck-Institut für Plasmaphysik, 85748 Garching, Germany*
[4)] *CEA, IRFM, F-13108 Saint-Paul-Lez-Durance, France*
[5)] *See the Appendix of F. Romanelli et al., Proceedings of the 25th IAEA Fusion Energy Conference 2014, Saint Petersburg, Russia*

(Dated: 12 August 2015)

Tungsten erosion in H-mode plasmas is quantified in the outer divertor of the JET ITER-Like Wall environment with optical emission spectroscopy on the 400.9 nm atomic neutral tungsten line. A novel cross-calibration procedure is developed to link slow, high spectral resolution spectroscopy and fast photomultiplier tube measurements in order to obtain ELM-resolved photon fluxes. Inter-ELM W erosion is exclusively impurity sputtering by beryllium because of the high sputter threshold for deuterons. Low beryllium concentrations resulted in low inter-ELM sputter yields of around 10^{-4} with respect to the total flux.

Intra-ELM W sources, which dominate the total W tungsten source, vary independently from the inter-ELM source. The amount of W erosion could only be partly explained by beryllium sputtering, indicating that during ELMs sputtering by fuel species is important. The total W outer divertor source is found to linearly increase with the power crossing the separatrix, whilst excessive divertor fueling can break this trend.

The influence of the W source rate on the tungsten content of the core plasma is investigated using Soft X-Ray emission to determine the tungsten content. At low source rates the content is determined by the source, but at higher source rates, other phenomena determine the total tungsten content. Indications of impurity flushing by ELMs is seen at ELM frequencies above approximately 40 Hz. The inner/outer divertor asymmetry of the W source during ELMs is investigated, and the outer divertor W source is larger by a factor of 1.8 ± 0.7.

I. INTRODUCTION

ITER will feature a full tungsten (W) divertor and a beryllium wall cladding[1]. This combination of a low-Z material for the main wall, and a refractory metal for the divertor, is selected to give a large operational flexibility as well as the capability to handle the large heat and particle fluxes to the divertor. In order to provide an integrated demonstration of the impact of this material combination, the JET tokamak is currently equipped with the ITER-Like Wall (ILW), which consists of solid beryllium limiters and cladding, as well as a combination of bulk W and W-coated carbon fiber composite divertor components[2–4].

Although material properties of W make it an ideal candidate for use in fusion reactors, there are stringent limits on the tolerable amount of W in the plasma core in view of radiative losses. An acceptable fusion performance is only attainable when the W core concentration is a few times 10^{-5} at most[5]. This low concentration requires on the one hand a minimization of the tungsten sources via detached divertor operation, and on the other hand the suppression of tungsten transport to the plasma core.

[a)] Electronic mail: N.denHarder@DIFFER.nl

Given these strict requirements on the tungsten core concentration, it is very important to get a complete understanding of the critical parameters for the erosion of tungsten components, notably the divertor. In this paper we will quantify the W sources in JET by optical emission spectroscopy under a wide range of H-mode plasmas. The emphasis is on the time dependence of the W source, so that the transient Edge Localized Modes are resolved, and the inter- and intra-ELM contributions can be distinguished. This is important because intra-ELM sources might show a different dependence on the plasma parameters, since the intra-ELM source may be linked to pedestal parameters rather than edge conditions. Also simulations indicate that a large fraction of the intra-ELM W-source might promptly redeposit, compared to the inter-ELM contribution[6]. In addition intra-ELM sources might be different in the efficiency with which the sputtered particles reach the core plasma, i.e. have a different divertor screening.

ELM-resolved W source information is obtained via a novel cross-calibration procedure between the 40 ms time resolution divertor spectroscopy and the 0.1 ms time resolution Photo Multiplier Tube (PMT) measurements through optical filters. Both spectroscopic methods look at neutral tungsten emission at 400.9 nm. Although the PMT measurements do provide a high time-resolution absolute photon flux, the signal is partially polluted because of non-W contributions passing through the nar-

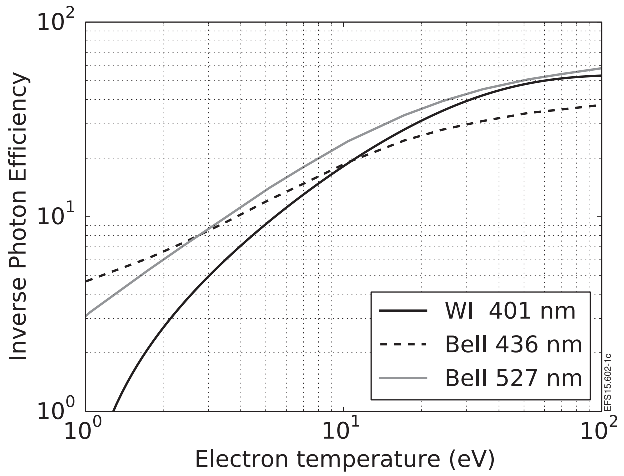

FIG. 1. The inverse photon efficiencies for the relevant spectral lines. The BeII $^S/_{XB}$ values were taken from ADAS[11], and the WI value was taken from Laengner *et al.*[10]

rowband filter. The degree of overestimation depends on the divertor conditions. With this calibration, these contributions are accounted for, and the W-source can be quantified with 0.1 ms time resolution. The inter-ELM W-source is then examined in terms of local plasma parameters. Impurities such as Be, C and O which can cause W sputtering are identified, and the measured sputter yield is compared with literature values as an additional consistency check. Sputtering species during ELMs are considered. The tungsten source per ELM is linked to pedestal parameters. The total intra-ELM source is discussed in relation to global physics parameters. Finally the tungsten core content is related to the tungsten source. Core contents and sources are used to calculate tungsten confinement times and study flushing of impurities by ELMs.

II. METHOD

Particle fluxes are derived from line-of-sight integrated absolute photon fluxes using the number of ionisations per emitted photon. This inverse photon efficiency is sometimes written as $^S/_{XB}$ because it has the form of an (ionization rate)/(branching ratio × excitation rate)[7,8]. Although high-Z elements are cumbersome to model, theoretical $^S/_{XB}$ data is available for W[9]. In this paper, experimentally derived $^S/_{XB}$ values for the WI transition at 400.9 nm were applied, which are widely used and agree well with theoretical data. The numerical value is based on results from several tokamaks[10]:

$$\frac{S}{XB}(T_e) = 53.7\left(1 - 1.04\exp\left(-\frac{T_e}{22.1}\right)\right) \quad (1)$$

For beryllium emission lines, $^S/_{XB}$ values for the experimental electron density range of of 10^{18} to 10^{20} m^{-3} were obtained from ADAS[11]. All inverse photon efficiencies used in this contribution are shown in Figure 1.

The T_e dependence of the $^S/_{XB}$ values necessitates the incorporation of an electron temperature measurement in the impurity flux determination. The divertor electron temperature in JET is measured by an array of Langmuir probes. The current-voltage characteristics of these flush mounted probes are fitted with a four parameter model, which gives an electron temperature as well as a total particle flux[12]. In the determination of the inter-ELM $^S/_{XB}$ values, the electron temperatures as measured by the probe system were used. During the ELMs, a fixed temperature of 100 eV was assumed, giving $^S/_{XB}$ values of 53 and 58 for the WI 401 nm and the BeII 527 nm emission lines. At temperatures above a few times ten electronvolts, the $^S/_{XB}$ values are only weakly dependent on the electron temperature, so the particle flux determination is not very sensitive to this assumption. If the electron temperature during ELMs would be 50 eV instead of the assumed 100 eV, the tungsten flux would be a 10 percent overestimation, and the beryllium flux would be overestimated by 15 percent.

Different systems are available to quantify divertor photon fluxes at JET. The KT3 system images optical emission from the divertor region via an optical mirror link system. The lines-of-sight have a toroidal extent of 2 mm and a poloidal size of 25 mm. Several spectrometers make up the KT3 system. The spectrometer equipped to study the WI emission is designated KT3B[13], a 0.75 meter Czerny-Turner spectrometer, which uses a 1200 lines/mm grating for the 400 nm wavelength range. Its 1024x1024 pixel Andor CCD camera, with 16-bit depth, was operated with exposure times of 40 ms.

The KS3 system uses fibre-optics to image the divertor[14]. The KS3 lines of sight are circular with a diameter of 33 mm, and cover the complete inner and outer divertor. Plasma emission is observed by Photo Multiplier Tubes through a filterscope to isolate the relevant spectral line. The KS3 system simultaneously monitors BeII emission at 436.1 nm, DI emission at 656.3 nm and WI emission. The average FWHM of the filters used to observe the WI 400.9 nm line is 0.89 ± 0.03 nm. The KS3 system was operated using exposure times of 0.1 ms.

The tungsten content of the plasma was calculated from the Soft X-Ray emission. The SXR emission is deconvolved, and the tungsten content is then calculated using electron temperature and density profiles in combination with the tungsten cooling factor known from literature[5].

III. RESULTS

A. Cross-calibration and ELM-resolved photon fluxes

In order to study W erosion ELM-resolved, fast WI photon fluxes needed, such as provided by the PMT system. However, the spectral resolution is poor since the

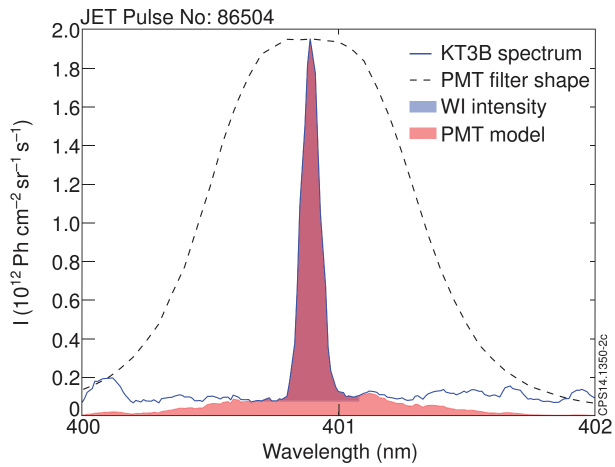

FIG. 2. The PMT filter shape is shown together with a KT3B spectrum. The area in red indicates the modeled PMT signal, which would in this case be an overestimation of the WI line intensity.

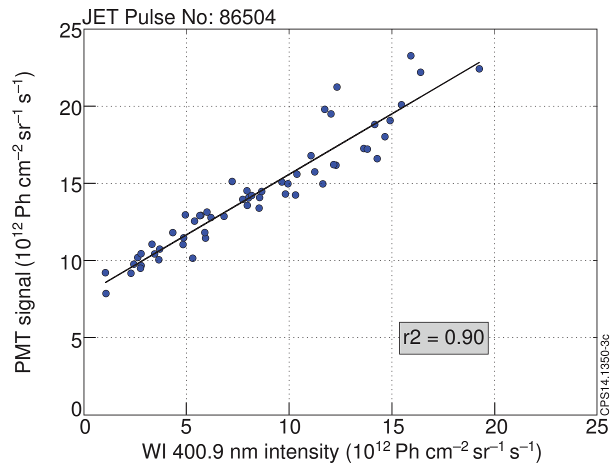

FIG. 3. Comparison between the WI line intensity and the observed PMT signal. A linear relation is found, although an appreciable part of the PMT signal is offset from background emission.

FWHM of the used filters are on the order of 1 nm. This leads to an overestimation of the tungsten signal due to contribution from the continuum background, as illustrated by Figure 2 in which a KT3B spectrum is overlaid with the KS3 filter shape.

To estimate the influence of background on the signal, we compared the WI line intensity determined with the KT3B spectrometer to the PMT signal over the flat top of several JET discharges. In this comparison the PMT data is time-integrated over the exposure windows of the spectrometer. A weighted sum of different KT3B poloidal channels is taken to match the PMT spatial resolution. Figure 3 shows the result of such comparison for the strikepoint location. In all the considered discharges, regardless of ELM frequency, there is a linear scaling between the WI line intensity and the PMT signal, but the PMT signal is consistently higher due to the background contribution. The majority of the offset observed in the PMTs is due to Bremsstrahlung. There is also additional background, possibly plasma light that is not completely attenuated by the filter. Notwithstanding the physics behind the fit parameters, a fit with a good coefficient of determination is a reliable way of reconstructing the WI line intensity from the PMT signal in combination with KT3B data. This cross-calibration yields the WI line intensity with a time resolution of 0.1 ms, sufficient to resolve individual ELMs.

Several discharges were investigated with the cross-calibration procedure. Only discharges with the strikepoint on the semi-horizontal outer divertor target plate were studied. Discharges for which the r2 of the fit was below 0.6 were excluded from further analysis. Since for a good fit quality a sufficiently large W photon flux was needed, these criteria resulted in a set of H-mode discharges with a significant amount of tungsten erosion. The set of discharges shows widely varying operating parameters, with the toroidal field strength ranging from 1.5 to 2.7 T, plasma currents from 1.5 to 2.5 MA, and heating powers between 5 and 23 MW.

To distinguish between the inter- and intra-ELM contribution, the ELMs need to be assigned. This was done based on the amplitude and derivative of the PMT signal. The sum of the inter- and intra-ELM contribution was compared with the integral of the PMT signal as additional check for the ELM assignment.

Emission of beryllium in the outer divertor is measured using a different PMT array with filters centered on the 527 nm emission line of singly ionized beryllium. A cross-calibration is not done for these signals, mainly since the beryllium emission is less localized, which makes it less straightforward to compare the PMT signals with spectroscopy data. If the background behaviour in the beryllium emission is similar to the tungsten background behaviour, the intra-ELM flux is accurate, while the inter-ELM flux will be an overestimation.

Since this procedure is only applicable on the outer divertor, where there is overlap between the spectrometer and filtered PMT observation chords, all sources given in this contribution are outer divertor sources, unless explicitly mentioned otherwise. Outer divertor particle fluxes are spatially integrated over the strikepoint and in the toroidal direction without taking into account shadowing effects or other toroidal asymmetries. In effect this assumes a global plasma-wetted fraction of 1.0. If there is shadowing, the plasma exposed part of the surface will catch a higher flux so that to first order the average surface flux is similar to the perfectly symmetric case.

B. Inter-ELM W sources and local plasma parameters

The main erosion mechanism for W in tokamaks is physical sputtering. Figure 4 shows the sputter yield for

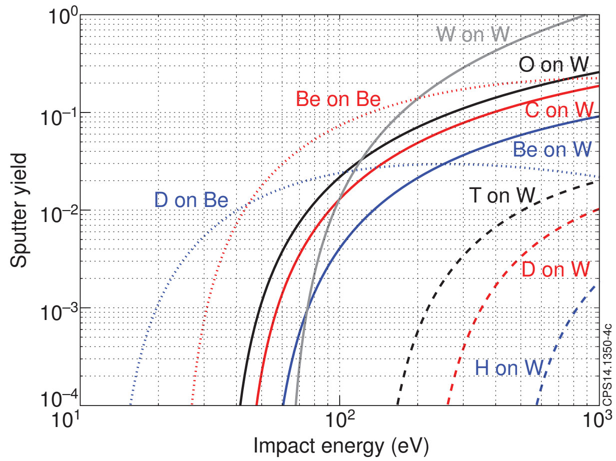

FIG. 4. Various sputter yields at normal incidence as function of the impact energy[15,16]. Because of the threshold behaviour, inter-ELM sputtering by fuel species will be negligible.

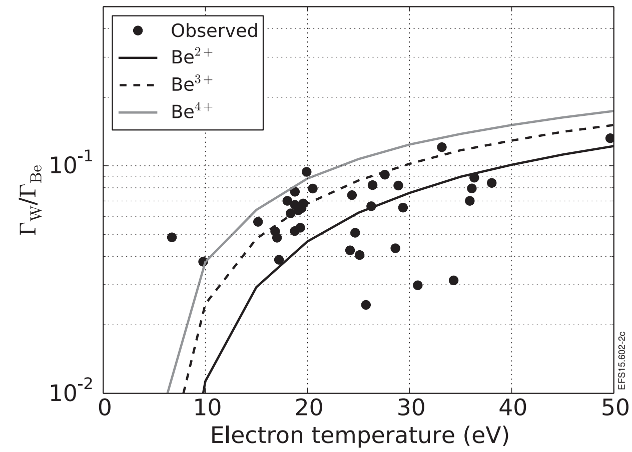

FIG. 5. Inter-ELM tungsten sputter yield by beryllium as function of the divertor electron temperature. Although there is some scatter in the measured sputter yields, the overall behaviour is indicative of W physical sputtering by beryllium.

various elements, calculated with the revised Bohdansky formula using ERO-TEXTOR data[15,16]. In JET a typical inter-ELM electron temperature is around 25 eV, and a typical particle flux is 10^{23} $m^{-2}s^{-1}$. Since the threshold energy for tungsten sputtering by deuterium is above 200 eV, only heavy impurities can sputter during the inter-ELM phase. In practice however, the incoming ions are not monoenergetic, and will carry $2kT_i$ to the wall, in addition to the $3Z_ikT_e$ due to acceleration through the Debye sheath[17]. In addition, not all particles will arrive at normal incidence. Averaging over the angular and energy distribution was performed as in references[16,18], which yields the sputter yield as function of electron temperature. The sputter yield for e.g. beryllium ions on tungsten then no longer shows clear threshold behaviour, although the threshold impact energy is 51 eV. Note that the angular distribution could be different than assumed, and this will have a significant effect on the sputter yield, as found by experiment and modeling[19,20]. The sputter yield can also be modified when surface layers are present[21]. Simulations of impurity migration show that layers of material are present at several locations in the JET divertor[22]. These effects however are neglected in this paper since the outer divertor is a net erosion zone, which means that the surface is most likely pristine tungsten[23].

Previously, in the JET ILW environment, in L-mode discharges beryllium was found as the dominant sputtering impurity[24]. Since there are no Be components in the divertor in the JET-ILW, all beryllium ions flowing into the divertor are from the main chamber[23]. Figure 5 shows the inter-ELM sputter yield in terms of the beryllium influx as function of electron temperature. Drawn in the Figure are the sputter yields for various charge states of beryllium. Measured sputter yields agree well with the literature values, which is a clear indication that sputtering by impurities other than beryllium is negligible. The main uncertainty in this measurement is the beryllium photon flux, which could be overestimated due to background emission. Correcting for this spurious signal would lower the beryllium flux, resulting in an increased sputter yield.

Relating the inter-ELM W sources to the total particle flux, i.e. including species which do not sputter, is commonly done to estimate the performance of operating scenarios in terms of wall erosion. For the studied discharges, effective sputter yields on the order of 10^{-4} are found. This is a result of the low impurity concentration, the beryllium fraction in the incoming particle flux is on the order of 10^{-3}. Figure 6 shows the effective sputter yield as function of divertor electron temperature. Clearly seen is that the sputter yield is lower at lower electron temperatures. This is mainly a result of the lower beryllium fraction in the total flux at these low electron temperatures.

C. Intra-ELM contribution to the W source

With the ELM-resolved signal it is possible to disentangle the inter- and intra-ELM contribution to the total W erosion, as shown in Figure 7. Since the studied discharges were not detached, and all have an electron temperature above 10 eV, the inter-ELM sources are relatively constant. The intra-ELM sources however vary over roughly one order of magnitude. For the H-mode discharges considered, the intra-ELM W source accounts for a large fraction of the total W source[25]. The intra-ELM source seems independent from the inter-ELM source. Note that the use of a constant $^{S}/_{XB}$ value could lead to an underestimation of the W-source, when the electron temperature excursion during an ELM is sufficient to lead to a higher $^{S}/_{XB}$ value for the intra-ELM photon flux. The ELM-resolved beryllium influxes

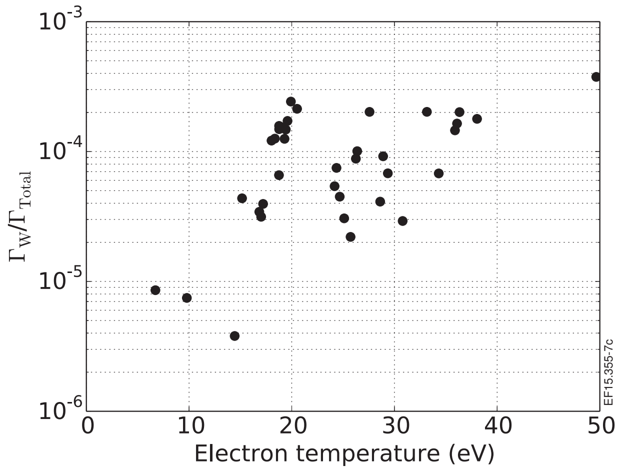

FIG. 6. Inter-ELM tungsten effective sputter yield as function of the divertor electron temperature as measured by probes. Because of the low beryllium concentration, the sputter yield in terms of total flux is low.

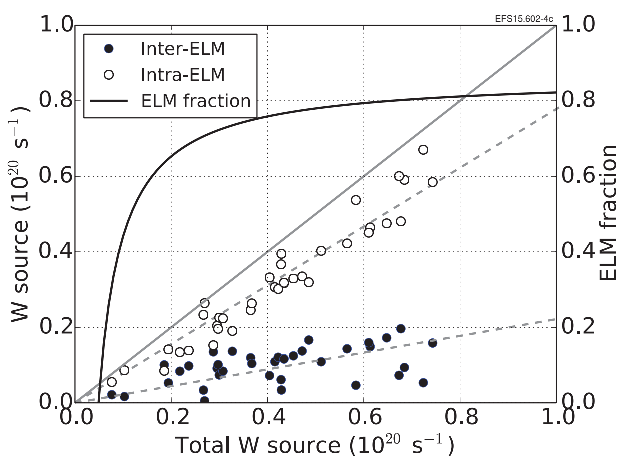

FIG. 7. Inter- and intra-ELM W outer divertor sources shown as function of the total W source. The inter-ELM sources are relatively constant, while the intra-ELM sources show a large variation. Already at a modest total source, the intra-ELM fraction is dominant.

show different behaviour, the inter-ELM flux dominates by approximately a factor of two, and the intra-ELM flux varies over about a factor of two.

The increase in WI emission during ELMs, a direct measure for the increase in erosion, had a time duration of 0.8 ± 0.1 ms, estimated from the temporal FWHM. Since this small time duration accounts for at least half of the tungsten source, the source strength during an ELM is strongly enhanced. While the inter-ELM tungsten influx is 9×10^{18} s^{-1}, during an ELM the W source is 5×10^{20} s^{-1} on average, a 60 fold increase.

The high source strength during ELMs is mainly caused by the increased temperature of the particles arriving at the divertor plates, which increases the sputter yield. The beryllium flux also increases during

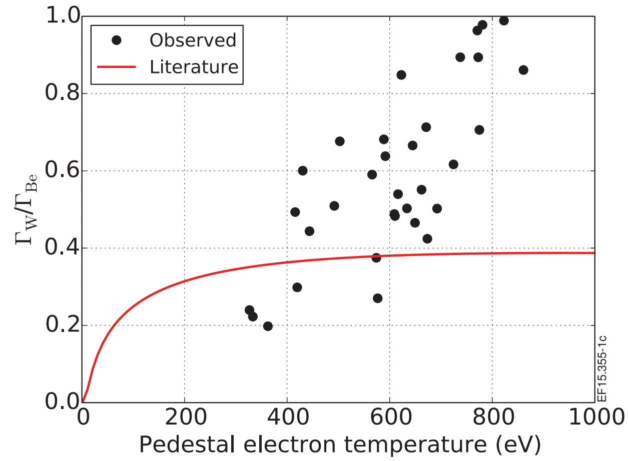

FIG. 8. The intra-ELM sputter yield of Be on W as function of the pedestal electron temperature. The red line indicates the literature sputter yield of fully ionized beryllium. Sputter yields above the red line indicate a contribution of fuel species to the sputtering.

ELMs, but only a factor of 2, although this could be slightly higher because of the overestimated inter-ELM flux. Since the Be on W sputter yield is known from literature as function of temperature, in principle an effective ELM ion temperature could be assigned on the basis of the observed sputter yield, assuming that beryllium is the only sputterer. However, because the sputter yield is almost constant at temperatures above a few hundred electronvolts, in practice this procedure is not feasible. Although the literature sputter yield is only weakly temperature dependent at ELM-relevant ion temperatures, the observed sputter yield shows variations, and at higher pedestal electron temperatures increases above the maximum sputter yield for beryllium on tungsten. The observed flux ratio between beryllium and tungsten is shown in Figure 8 together with the literature sputter yield for fully ionized beryllium ions on tungsten. Since at higher pedestal electron temperatures the observed sputter yields exceeds the literature yield, sputtering by beryllium alone cannot explain the observed tungsten source. This indicates that at increased pedestal temperatures, sputtering by fuel species becomes important. This behaviour is already expected from literature sputter yields shown in Figure 4, combined with an educated guess on the divertor plasma parameters during an ELM.

D. Intra-ELM W sources and pedestal parameters

Since during ELMs particles are transported from the hot pedestal region to the target plates, it is instructive to analyze the intra-ELM W source as function of pedestal parameters. Figure 9 shows the average tungsten source for individual ELMs as function of the confined energy loss for various fueling rates. Different majority gas fueling rates in units of electrons per second are indicated

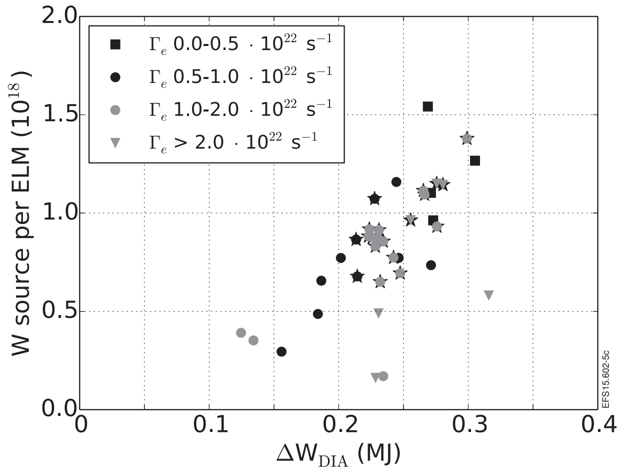

FIG. 9. The average W outer divertor source per ELM shown as function of the drop of diamagnetic energy during an ELM for several fueling rates. RF-heated shots are indicated with a star. In pulses with a similar fueling, the W ELM source show a linear dependence on the energy loss.

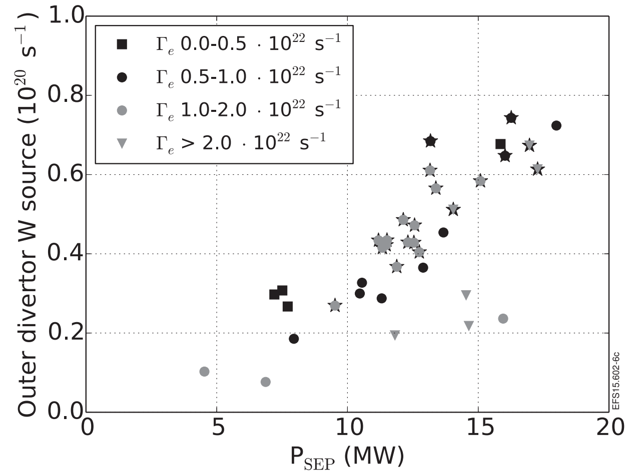

FIG. 10. Total W outer divertor sources shown as function of the power crossing the separatrix for several fueling rates. RF-heated shots are indicated with a star. In pulses with a similar fueling, W sources shows a linear dependence on P_{SEP}, through the increased ELM frequency at higher P_{SEP}.

with different colours. Pulses with at least half a MW of ICRH during the flat top phase are indicated with a star. This figure shows that low fueling rates lead to larger ELMs, which gives a high W source per ELM[26]. However, this is offset by the low ELM frequency, so that the total W influx can still be low. High fueling rates lead to a lower W influx per ELM, although the energy loss per ELM is not necessarily smaller.

E. Total W sources and global physics parameters

Although the limited number of studied pulses prohibits a rigorous scaling analysis, some global physics parameters clearly correlate with the observed W-source. Note that although these global quantities can obscure the underlying physics, these correlations are still useful from an operational point of view. Of the studied parameters, the power crossing the separatrix shows the most convincing correlation. Figure 10 shows, for several JET pulses, the total W-source as function of the power crossing the separatrix which is calculated as: $P_{SEP} = P_{NBI} + P_{ICRH} + P_{Ohmic} - dW_{DIA}/dt - P_{Rad,bulk}$. For a given fueling rate, the W source linearly increases with power crossing the separatrix. Fueling above 10^{22} s^{-1} does decrease the W source, but low fueling does not lead to a highly increased W source. Pulses with ICRH show in general a higher W outer divertor source, but the overall effect is small. ICRH is expected to increase the W influx because of RF induced sheath effects[27,28]. The correlation between the W sources and P_{SEP} is mainly the result the increased ELM frequency at higher P_{SEP}. For type I ELMs, the energy loss per ELM does not vary significantly with heating power, but the ELM frequency increases as P_{SEP} increases, due to a faster build up of the edge pressure gradient[29].

F. W sources and plasma W content

Relating the ELM-resolved tungsten sources with the tungsten content of the plasma could give insight in the combined effects of divertor screening and pedestal transport. Divertor screening is expected to be high, PIC calculations indicate that the promptly redeposited fraction of the eroded tungsten will exceed 97 percent even in the most favourable conditions, and during ELMs the redeposited fraction will be higher still[6]. Although it will be difficult to single out the effect of redeposition on the global tungsten content of the plasma, it is instructive to evaluate the tungsten content in terms of the tungsten source.

As shown in Figure 11, the total W content shows a weak dependence on the source below source rates of 0.4×10^{20} s^{-1}. The large spread in the data is an indication that although the source rate plays a small role, transport phenomena are more important for the tungsten content of the main plasma. The ratio between the total W content and the total source can be used to estimate an effective confinement time or penetration factor of the tungsten ions[30,31]. Since here this factor is calculated in terms of only the outer divertor source, the tungsten confinement time will be lower in practice. Tungsten confinement times in the range from 1 to 10 ms were found, which is comparable to results obtained in JET by Fedorczak *et al.*[32].

The tungsten confinement time shows a dependence on the ELM frequency, decreasing when the ELM frequency is higher. However, since the source is proportional to the ELM frequency, and the total tungsten content does

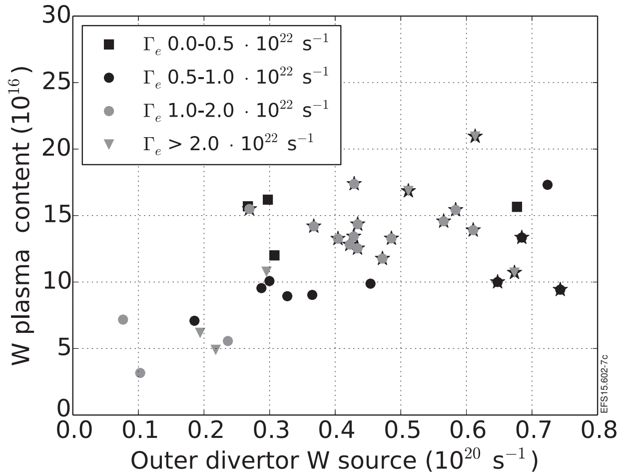

FIG. 11. The total W content of the plasma as function of the total W outer divertor source. RF-heated shots are indicated with a star. There is some correspondence between the tungsten source rate and the core concentration, but the large scatter indicates that other processes are at play as well.

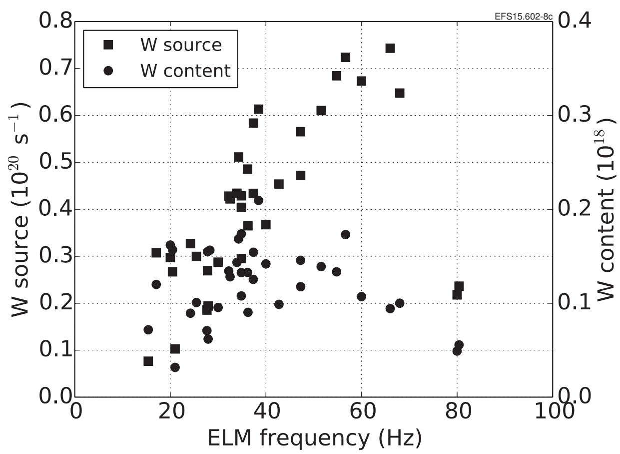

FIG. 12. The total W content of the plasma and the outer divertor tungsten source as function of the ELM frequency. Despite the large scatter, above an ELM frequency of about 40 Hz, the tungsten content of the plasma stabilizes while the source still increases. This can be interpreted as a sign of ELM flushing.

not show large variations, the observed variation in confinement time is mostly attributed to variations in the W source. Both quantities are plotted as function of the ELM frequency in Figure 12. An increased ELM frequency leads to an increased source, except at the highest ELM frequency where the ELM signature is fuzzy. The tungsten content of the plasma increases with the source at low ELM frequencies, but around 40 Hz this trend reverses and the content decreases, in contrast with the source which still increases. This is a sign of flushing of W out of the main plasma by ELMs[32,33]. This is in line with observations that low ELM frequencies often leads to a high core radiation levels[34].

G. Inner and outer divertor contributions

The inner and outer divertor PMT signals were compared in order to estimate the relative contribution of the inner and outer divertor W source. To compare the signals on an equal footing, no cross-calibration was performed, hence the inter-ELM sources could not be studied. The outer divertor W source is larger during ELMs by a factor of 1.8 ± 0.7. Given the scatter in the data, no systematic dependencies could be found. An asymmetry in ELM energy loads by a factor of about 2 was found previously in JET. Whether the inner or outer divertor is favoured is dependent on the direction of the ion $\mathbf{B} \times \nabla \mathbf{B}$ drift[35].

IV. CONCLUSION

W sources were studied in the JET ITER-Like Wall environment with optical emission spectroscopy for the C33 campaign. A cross-calibration method was developed to link fast PMT measurements with 40 ms time resolution spectra to obtain 0.1 ms resolution WI photon fluxes. Inter-ELM W erosion was found to be dominated by the impurity beryllium. Of the total flux, the beryllium fraction is on the order of 10^{-3}, which resulted in effective sputter yields on the order of 10^{-4}. These results are similar to earlier findings in L-mode discharges[24].

Intra-ELM erosion was found to dominate the total W source. The intra-ELM source varied over one order of magnitude while the inter-ELM source remained approximately the same, making ELM control an important priority when considering the total W source. Sputtering during ELMs can be largely explained by beryllium sputtering, although at higher pedestal electron temperatures sputtering by fuel species becomes significant.

Larger ELMs in terms of pedestal energy loss were found to give a larger tungsten source per ELM. The total tungsten source correlates well with P_{SEP}, mainly due to the increased ELM frequency at higher P_{SEP}.

Although some correspondence was seen between the tungsten source and the total tungsten content of the plasma, the large spread in the data is an indication that although the source rate plays a small role, transport phenomena are more important for the core content. Tungsten confinement times calculated on basis of the total tungsten content and the outer divertor source were between 1 and 10 ms. In discharges with type I ELMs, the source increases with increasing ELM frequency. This contrasts with the plasma tungsten content, which increases with the source until at an ELM frequency of approximately 40 Hz the trend reverses and the content decreases while the source is still increasing. This was interpreted as a sign of ELM flushing.

Inner and outer divertor sources were compared on the basis of the total photon flux. Intra-ELM fluxes were found to be asymmetric, with the outer divertor favoured by a factor of 1.8 ± 0.7.

V. ACKNOWLEDGEMENTS

This work has been carried out within the framework of the EUROfusion Consortium and has received funding from the Euratom research and training programme 2014-2018 under grant agreement No 633053. The views and opinions expressed herein do not necessarily reflect those of the European Commission.

[1] R. A. Pitts, A. Kukushkin, A. Loarte, A. Martin, M. Merola, C. E. Kessel, V. Komarov, and M. Shimada. Status and physics basis of the ITER divertor. *Physica Scripta*, 2009(T138):014001, 2009.

[2] G. F. Matthews, P. Edwards, T. Hirai, M. Kear, A. Lioure, P. Lomas, A. Loving, C. Lungu, H. Maier, P. Mertens, D. Neilson, R. Neu, J. Pamela, V. Philipps, G. Piazza, V. Riccardo, M. Rubel, C. Ruset, E. Villedieu, M. Way, and the ITER-like Wall Project Team. Overview of the ITER-like wall project. *Physica Scripta*, 2007(T128):137, 2007.

[3] G. F. Matthews, M. Beurskens, S. Brezinsek, M. Groth, E. Joffrin, A. Loving, M. Kear, M-L Mayoral, R. Neu, P. Prior, V. Riccardo, F. Rimini, M. Rubel, G. Sips, E. Villedieu, P. de Vries, M. L. Watkins, and EFDA-JET contributors. JET ITER-like wall – overview and experimental programme. *Physica Scripta*, 2011(T145):014001, 2011.

[4] R. Neu, A. Kallenbach, M. Balden, V. Bobkov, J. W. Coenen, R. Drube, R. Dux, H. Greuner, A. Herrmann, J. Hobirk, H. Hoehnle, K. Krieger, M. Kocan, P. Lang, T. Lunt, H. Maier, M. Mayer, H. W. Müller, S. Potzel, T. Pütterich, J. Rapp, V. Rohde, F. Ryter, P. A. Schneider, J. Schweinzer, M. Sertoli, J. Stober, W. Suttrop, K. Sugiyama, G. van Rooij, M. Wischmeier, and ASDEX Upgrade Team. Overview on plasma operation with a full tungsten wall in ASDEX Upgrade. *Journal of Nuclear Materials*, 438(S):S34–S41, JUL 2013. 20th International Conference on Plasma-Surface Interactions in Controlled Fusion Devices (PSI), Forschungszentrum Julich, Aachen, GERMANY, MAY 21-25, 2012.

[5] T. Pütterich, R. Neu, R. Dux, A.D. Whiteford, M.G. O'Mullane, H.P. Summers, and the ASDEX Upgrade Team. Calculation and experimental test of the cooling factor of tungsten. *Nuclear Fusion*, 50(2):025012, 2010.

[6] D. Tskhakaya and M. Groth. Modelling of tungsten re-deposition coefficient. *Journal of Nuclear Materials*, (0):–, 2014.

[7] K.H. Behringer. Spectroscopic studies of plasma-wall interaction and impurity behaviour in tokamaks. *Journal of Nuclear Materials*, 145-147(0):145–153, 1987.

[8] K. Behringer, H. P. Summers, B. Denne, M. Forrest, and M. Stamp. Spectroscopic determination of impurity influx from localized surfaces. *Plasma Physics and Controlled Fusion*, 31(14):2059, 1989.

[9] I. Beigman, A. Pospieszczyk, G. Sergienko, I. Yu Tolstikhina, and L. Vainshtein. Tungsten spectroscopy for the measurement of W-fluxes from plasma facing components. *Plasma Physics and Controlled Fusion*, 49(11):1833, 2007.

[10] M. Laengner, S. Brezinsek, J.W. Coenen, A. Pospieszczyk, D. Kondratyev, D. Borodin, H. Stoschus, O. Schmitz, V. Philipps, and U. Samm. Penetration depths of injected/sputtered tungsten in the plasma edge layer of TEXTOR. *Journal of Nuclear Materials*, 438(0):S865–870, 2013.

[11] H. P. Summers. *The ADAS User Manual, version 2.6 http://www.adas.ac.uk*, 2004.

[12] J. P. Gunn, C. Boucher, B. L. Stansfield, and S. Savoie. Flush-mounted probes in the divertor plates of Tokamak de Varennes. *Review of Scientific Instruments*, 66(1):154–159, 1995.

[13] A. Meigs, M. Stamp, R. Igreja, S. Sanders, P. Heesterman, and JET-EFDA Contributors. Enhancement of JET's mirror-link near-ultraviolet to near-infrared divertor spectroscopy system. *Review of Scientific Instruments*, 81(10):–, 2010.

[14] P. D. Morgan, K. H. Behringer, P. G. Carolan, M. J. Forrest, N. J. Peacock, and M. F. Stamp. Spectroscopic measurements on the Joint European Torus using optical fibers to relay visible radiation. *Review of Scientific Instruments*, 56(5):862–864, 1985.

[15] C. García-Rosales, W. Eckstein, and J. Roth. Revised formulae for sputtering data. *Journal of Nuclear Materials*, 218(1):8 – 17, 1995.

[16] A. Kirschner, V. Philipps, J. Winter, and U. Kögler. Simulation of the plasma-wall interaction in a tokamak with the Monte Carlo code ERO-TEXTOR. *Nuclear Fusion*, 40(5):989, 2000.

[17] P.C . Stangeby. Taylor & Francis, 2000.

[18] V.A. Abramov, Yu.L. Igitkhanov, V.I. Pistunovich, and V.A. Pozharov. First wall and divertor plate sputtering in a tokamak reactor. *Journal of Nuclear Materials*, 162164(0):462–466, 1989.

[19] K. Schmid, M. Mayer, C. Adelhelm, M. Balden, S. Lindig, and the ASDEX Upgrade team. Impact of gyro-motion and sheath acceleration on the flux distribution on rough surfaces. *Nuclear Fusion*, 50(10):105004, 2010.

[20] D. Borodin, S. Brezinsek, J. Miettunen, M. Stamp, A. Kirschner, C. Björkas, M. Groth, S. Marsen, C. Silva, S. W. Lisgo, D. Matveev, M. Airila, V. Philipps, and The JET-EFDA Contributors. Determination of Be sputtering yields from spectroscopic observations at the JET ITER-like wall based on three-dimensional ERO modelling. *Physica Scripta*, 2014(T159):014057, 2014.

[21] I. Bizyukov and K. Krieger. Transition from tungsten erosion to carbon layer deposition with simultaneous bombardment of tungsten by helium and carbon. *Journal of Applied Physics*, 101(10):–, 2007.

[22] K. Schmid, K. Krieger, S. W. Lisgo, G. Meisl, S. Brezinsek, and JET Contributors. WALLDYN simulations of global impurity migration in JET and extrapolations to ITER. *Nuclear Fusion*, 55(5):053015, 2015.

[23] S. Brezinsek and JET-EFDA contributors. Plasma-surface interaction in the Be/W environment: Conclusions drawn from the JET-ILW for ITER. *Journal of Nuclear Materials*, (0):–, 2014.

[24] G. J. van Rooij, J. W. Coenen, L. Aho-Mantila, S. Brezinsek, M. Clever, R. Dux, M. Groth, K. Krieger, S. Marsen, G. F. Matthews, A. Meigs, R. Neu, S. Potzel, T. Pütterich, J. Rapp, and M. F. Stamp. Tungsten divertor erosion in all metal devices: Lessons from the ITER like wall of JET. *Journal of Nuclear Materials*, 438, Supplement:S42 – S47, 2013. Proceedings of the 20th International Conference on Plasma-Surface Interactions in Controlled Fusion Devices.

[25] C. Giroud, G. P. Maddison, S. Jachmich, F. Rimini, M. N. A. Beurskens, I. Balboa, S. Brezinsek, R. Coelho, J. W. Coenen, L. Frassinetti, E. Joffrin, M. Oberkofler, M. Lehnen, Y. Liu, S. Marsen, K. McCormick, A. Meigs, R. Neu, B. Sieglin, G. van Rooij, G. Arnoux, P. Belo, M. Brix, M. Clever, I. Coffey, S. Devaux, D. Douai, T. Eich, J. Flanagan, S. Grünhagen, A. Huber, M. Kempenaars, U. Kruezi, K. Lawson, P. Lomas, C. Lowry, I. Nunes, A. Sirinnelli, A. C. C. Sips, M. Stamp, S. Wiesen, and JET-EFDA contributors. Impact of nitrogen seeding on confinement and power load control of a high-triangularity jet elmy h-mode plasma with a metal wall. *Nuclear Fusion*, 53(11):113025, 2013.

[26] C. Guillemaut, A. Jardin, J. Horacek, A. Autricque, G. Arnoux, J. Boom, I. Borodkina, S. Brezinsek, J. W. Coenen, E. De La Luna, S. Devaux, T. Eich, D. Harting, A. Kirschner, B. Lipschultz, G. F. Matthews, A. Meigs, D. Moulton, M. OMullane, M. Stamp, and JET contributors. Experimental estimation of tungsten impurity sputtering due to Type I ELMs in JET-ITER-like Wall. *Physica Scripta*, 2015.

[27] F. W. Perkins. Radiofrequency sheaths and impurity generation by icrf antennas. *Nuclear Fusion*, 29(4):583, 1989.

[28] E. Lerche, M. Goniche, P. Jacquet, D. Van Eester, V. Bobkov, L. Colas, C. Giroud, I. Monakhov, F. Rimini, C. Angioni, M. Baruzzo, T. Blackman, S. Brezinsek, M. Brix, F. J. Casson, A. Czarnecka, K. Crombé, C. Challis, R. Dumont, J. Eriksson, N. Fedorczak, M. Graham, J. Graves, G. Gorini, J. Ho-

birk, E. Joffrin, T. Johnson, Y. Kazakov, V. Kiptily, A. Krivska, M. Lennholm, P. Lomas, C. Maggi, P. Mantica, G. Mathews, M. L. Mayoral, L. Meneses, J. Mlynar, P. Monier-Garbet, M. F. Nave, C. Noble, M. Nocente, I. Nunes, J. Ongena, G. Petravich, V. Petrzilka, T. Pütterich, M. Reich, M. Santala, E. R. Solano, A. Shaw, G. Sips, M. Stamp, M. Tardocchi, M. Tsalas, M. Valisa, and JET Contributors. ICRH for core impurity control in JET-ILW. *Nuclear Fusion*, 2015.

[29] H. Zohm. Edge Localized Modes (ELMs). *Plasma Physics and Controlled Fusion*, 38(2):105, 1996.

[30] B. Lipschultz, D.A. Pappas, B. LaBombard, J.E. Rice, D. Smith, and S.J. Wukitch. A study of molybdenum influxes and transport in Alcator C-Mod. *Nuclear Fusion*, 41(5):585, 2001.

[31] R. Dux, A. Janzer, T. Pütterich, and ASDEX Upgrade Team. Main chamber sources and edge transport of tungsten in H-mode plasmas at ASDEX Upgrade. *Nuclear Fusion*, 51(5):053002, 2011.

[32] N. Fedorczak, P. Monier-Garbet, T. Pütterich, S. Brezinsek, P. Devynck, R. Dumont, M. Goniche, E. Joffrin, E. Lerche, B. Lipschultz, E. de la Luna, G. Maddison, C. Maggi, G. Matthews, I. Nunes, F. Rimini, E.R. Solano, P. Tamain, M. Tsalas, P. de Vries, and JET-EFDA contributors. Tungsten transport and sources control in JET ITER-like wall H-mode plasmas. *Journal of Nuclear Materials*, (0):–, 2014.

[33] Tungsten screening and impurity control in jet. 2012. Proceedings of the 24th IAEA Fusion Energy Conference.

[34] Plasma operation with an all metal first-wall: Comparison of an ITER-like wall with a carbon wall in JET. *Journal of Nuclear Materials*, 438, Supplement:S2 – S10], year = 2013, note = Proceedings of the 20th International Conference on Plasma–Surface Interactions in Controlled Fusion Devices, issn = 0022–3115, doi = 10.1016/j.jnucmat.2013.01.282, url = http://www.sciencedirect.com/science/article/pii/S0022311513002900, author = G.F. Matthews.

[35] T. Eich, A. Kallenbach, R. A. Pitts, S. Jachmich, J. C. Fuchs, A. Herrmann, and J. Neuhauser. Divertor power deposition and target current asymmetries during type-1 ELMS in ASDEX Upgrade and JET. *Journal of Nuclear Materials*, 363–365:989–993, 2007.

VI. SUPPLEMENTARY INFORMATION

JET Pulse Number	t_{start} (s)	t_{end} (s)
86504	49.20	51.50
86523	44.90	46.00
86524	45.10	47.00
86529	45.00	46.00
86530	45.00	46.00
86531	47.20	48.00
86532	46.50	48.10
86533	49.80	51.55
86534	49.80	51.55
86535	49.80	51.10
86536	49.80	51.55
86537	49.80	50.95
86538	49.80	51.60
86581	53.30	56.40
86638	50.15	51.05
86683	49.00	49.90
86684	49.00	51.45
86689	49.00	52.50
86692	59.30	60.95
86694	59.30	60.90
86696	59.30	60.90
86699	59.70	60.64
86703	60.70	62.70
86717	45.80	47.00
86718	46.35	47.50
86719	46.05	47.50
86882	59.80	60.90
86885	59.60	60.90
86929	53.80	56.00
87043	53.70	55.40
87044	53.80	55.30
87124	53.75	55.90
87160	48.80	53.60
87161	48.80	53.20
87162	48.80	53.80
87163	48.80	52.20
87164	48.80	52.80
87167	48.80	52.80
87168	48.80	52.00
87169	48.70	52.00
87171	48.70	50.00

TABLE I. List of all the JET pulses considered in this contribution.